Homogeneous record of Atlantic hurricane surge threat since 1923

Aslak Grinsted[a,1,2], John C. Moore[a,b,c], and Svetlana Jevrejeva[a,d]

[a]State Key Laboratory of Earth Surface Processes and Resource Ecology, College of Global Change and Earth System Science, Beijing Normal University, Beijing 100875, China; [b]Arctic Centre, University of Lapland, FI-96101 Rovaniemi, Finland; [c]Department of Earth Sciences, Uppsala University, SE-75236 Uppsala, Sweden; and [d]National Oceanography Centre, Liverpool L3 5DA, United Kingdom

Detection and attribution of past changes in cyclone activity are hampered by biased cyclone records due to changes in observational capabilities. Here we construct an independent record of Atlantic tropical cyclone activity on the basis of storm surge statistics from tide gauges. We demonstrate that the major events in our surge index record can be attributed to landfalling tropical cyclones; these events also correspond with the most economically damaging Atlantic cyclones. We find that warm years in general were more active in all cyclone size ranges than cold years. The largest cyclones are most affected by warmer conditions and we detect a statistically significant trend in the frequency of large surge events (roughly corresponding to tropical storm size) since 1923. In particular, we estimate that Katrina-magnitude events have been twice as frequent in warm years compared with cold years ($P < 0.02$).

climate | extreme | hazard | risk | flood

The relationship between global warming and Atlantic hurricane activity is a controversial topic (1–3). Some have linked cyclone activity to sea surface temperatures in the cyclogenesis region (2, 4). Other competing hypotheses include teleconnections with El Niño–Southern Oscillation (5), North Atlantic Oscillation (6–8), Atlantic Multidecadal Oscillation (6), tropical temperatures (3, 9), and Sahel drought (10). Whereas others note that bias in the observational record casts doubt on any statistical power from the relationship (11). Estimating and correcting the historical bias hamper assessment of the links between tropical cyclone activity and climate change (1, 2, 11, 12). Hence, any discussion of observational links or causality between global mean temperatures and hurricane impacts relies on an unbiased estimate of hurricanes as a function of time. There is a rising trend over the 20th century in the observed numbers of Atlantic tropical cyclones (1, 12). However, observational methods have improved over time, especially since the satellite era, but also after airborne observations became commonplace; therefore some cyclones were missed in the past.

Most efforts have focused on estimating total Atlantic cyclone activity rather than the number of land-falling storms. This is because relatively few storms make land, and small changes in storm tracks can make a difference between a landfall and a near miss. However, from the economic damage perspective the hurricanes that remain far away from shore in the Atlantic are much less important than those closer to land. Hence in constructing an unbiased record of storms we need to ask what we want to measure. The strong winds and intense low pressure associated with tropical cyclones generate storm surges. These storm surges are the most harmful aspect of tropical cyclones in the current climate (1, 12), and wherever tropical cyclones prevail they are the primary cause of storm surges. A measure of storm surge intensity would therefore be a good candidate measure of cyclone potential impact.

In this paper we construct such a record, using long-term tide-gauge records from stations that have been operational for much longer than the satellite era. These provide a consistent dataset for examining hurricanes affecting the southeastern United States. We also show that the index is actually dominated by land-falling hurricanes rather than winter storms and that the

index reflects economic damage. Rather than a simple number count of cyclones, we produce a yearly probability distribution of storm surge intensity. We then apply a robust method of estimating confidence intervals to the frequency of extreme events. Finally we show that there is a difference in frequency of cyclones between cold and warm years and that the effect is strongest for the larger cyclones and hurricanes.

Results

We wish to produce a long-term, homogeneous record of storm surge activity. Tide gauges are very suitable as they are simple devices that have been used for hundreds of years to measure sea level. We define the region of interest to be the western Atlantic between 10°N and 40°N. This leaves us with the six tide gauges from the region of interest (Fig. 1, *Inset* and Fig. S1) with the main criteria that we wanted to construct a homogeneous record that covered the great 1926 storm surge (13) and the general high cyclone activity of the 1930s. Here, we use data from the Research Quality Data Set (RQDS) (14). The RQDS records are extended to the present using fast delivery data from the global sea level observing system (14) and in a single instance (Mayport, FL) using preliminary water-level data from the National Oceanic and Atmospheric Administration (NOAA) Center for Operational Oceanographic Products and Services (15). We manually screen the data quality of the Mayport preliminary water-level data before down-sampling. We then proceed to filter these records to enhance the storm signal while reducing the signals due to instrument changes, harbor development, and erroneous time shifts in the records.

Tropical cyclones are highly localized. However, over time the sea-level disturbance will dissipate. Daily averages increase the storm footprint to hundreds of kilometers, which means that relatively few tide-gauge stations provide adequate coverage. Large storms can also produce extreme sea levels that can be seen in tide-gauge records for several days. The potential energy stored in a sea-level perturbation is related to the square of the vertical displacement of the sea surface (16); hence we use squared day-to-day difference in local sea level. Daily data are insensitive to harbor development and changes in measurement methods, which can strongly affect high-frequency variability such as significant wave height. Day-to-day differencing further minimizes tidal influence and slowly varying trends from, e.g., rising global sea levels (17).

We observe that summer sea level is relatively calm except for the sporadic and obvious influence from cyclones, whereas winters have a higher degree of background variability. We therefore

Fig. 1. (A) Average surge index over the cyclone season. (B) Observed frequency of surge events with surge index greater than 10 units/y (surge index > 10 units) and linear trend (black). (C) Accumulated cyclone energy for US landfalling storms. (D) Annual average global mean surface temperature anomaly from GISTEMP (23), shaded to show warmer and colder than median temperatures. Thick lines in A, B, and C are 5-y moving averages. *Inset* in A shows locations of the six tide gauges used in the construction of the surge index.

remove the background annual cycle by division. This also brings the records to a common normalized reference that removes local effects due to, e.g., bathymetry (16). We call the multistation daily maximum of deseasonalized squared day-to-day differences the surge index. These processing steps are outlined in more detail in *SI Methods*, section S1, Fig. S2, and Table S1.

To visualize the surge index and facilitate comparisons to other measures of cyclone activity we have down-sampled the surge index to annual resolution. We do this in two ways (Fig. 1 *A* and *B*): The first way is the average value over the hurricane season

(which we here define as July–November) and the second way is a measure of the annual frequency of extreme events above a threshold corresponding to five to six events per year.

Discussion

In this section we demonstrate that the surge index primarily records surge threat from tropical cyclones. We compare the new surge index with several common measures of tropical cyclone activity, most of them derived from the Atlantic Hurricane Database (HURDAT; ref. 18) with wind speed corrections as detailed in ref. 2: tropical cyclone counts for various magnitude thresholds on the Saffir–Simpson scale, accumulated cyclone energy (ACE) (19), net tropical cyclone activity (NTC) (20), and power dissipation index (PDI). We also calculate several of these measures restricted to storms making US landfall. These we denote with a US prefix (e.g., US-ACE). Additionally, we compare the surge index with the "PL05" normalized hurricane damage (NHD) from Pielke et al. (21).

As an example we show the daily surge index compared with ACE and US-ACE for the very active 2005 season (Fig. 2). The ACE is traditionally defined as an annually integrated value. Here, we have made the natural extension of this definition to a daily integrated value. It is clear that the surge index is particularly sensitive to hurricanes making landfall, which supports the interpretation that the surge index is closely related to the actual threat.

Table 1 shows the correlation of the seasonal surge index with other measures. The surge index is positively correlated with all of the comparison measures. The best correlations are found with measures that emphasize intensity (e.g., NTC, ACE, and PDI) and measures that are restricted to US land-falling storms only. Table 1 also shows that low-frequency correlation tends to be at a higher level than the year-to-year correlation. This is to be expected given that there are low-frequency driving agents related to various climate forcings (4, 8). One notable exception is NHD, which shows poor low-frequency correlations. However, NHD has been subjected to extensive corrections for inflation and changes in societal conditions over time (21). These corrections affect primarily low-frequency signals and trends and we interpret the poor low-frequency correlation with surge index to be due to a substantial remaining bias in NHD. We therefore consider the low-frequency variability (i.e., trend) of NHD suspect. We note, however, that the surge index does capture the high-frequency variability in NHD, thus supporting the interpretation that it is truly a proxy for cyclone threat. It is conceivable that the surge index could be used to correct for the remaining bias in NHD.

In Table S2 we show the surge index of the 50 greatest events. The surge index ranking reflects the impact at the specific tide-gauge locations and therefore should not be interpreted as a storm ranking. The purpose of this list is to demonstrate that the surge index truly captures cyclone activity, rather than provide a storm severity ranking. A few events outside the hurricane season cannot be attributed to tropical cyclones. Several of these

Fig. 2. Comparison of the surge index (blue) with ACE (light red) and US-ACE (red) for the 2005 hurricane season.

Table 1. Correlations between July–November surge index and other measures of cyclone activity

Series	Period of overlap	Correlation full period	Correlation 1950–2005	High-frequency correlation	Low-frequency correlation
Cat 0–5	1923–2008	0.56	0.65	0.51	0.64
Cat 1–5	1923–2008	0.55	0.57	0.54	0.56
Cat 2–5	1923–2008	0.50	0.42	0.51	0.50
Cat 3–5	1923–2008	0.51	0.47	0.42	0.58
Cat 4–5	1923–2008	0.53	0.50	0.46	0.62
Cat 5	1923–2008	0.38	0.61	0.41	0.48
US cat 0–5	1923–2008	0.54	0.55	0.55	0.56
US cat 1–5	1923–2008	0.57	0.57	0.55	0.67
US cat 2–5	1923–2008	0.55	0.56	0.51	0.66
US cat 3–5	1923–2008	0.57	0.60	0.55	0.67
US cat 4–5	1923–2008	0.61	0.70	0.57	0.74
US cat 5	1923–2008	0.38	0.62	0.38	0.46
ACE	1923–2008	0.61	0.58	0.54	0.72
US ACE	1923–2008	0.58	0.58	0.51	0.77
NTC	1923–2006	0.58	0.55	0.48	0.54
PDI	1923–2008	0.60	0.58	0.53	0.73
US PDI	1923–2008	0.58	0.61	0.52	0.75
NHD	1923–2005	0.65	0.66	0.59	0.38

Low-frequency correlation is the correlation of the two series after a 5-y moving average. High-frequency correlation is the correlation of the residuals after subtracting this moving average. A US prefix indicates that the metric has been restricted to US-landfalling storms only. Cat, category.

events, however, show up in other records of extreme weather; e.g., the large March 13, 1993 event is commonly known as the 1993 superstorm (22).

The surge index can be interpreted as a potential threat to infrastructure. A large surge does not necessarily mean that the associated storm caused a lot of damage. It depends on the detailed conditions of when and where the storm hit the coast. We argue that the surge index is a more direct measure of threat than most of the HURDAT-derived measures. Large surge index values are a manifestation of what the storm is able to do exactly at the time of landfall. Other measures, such as integrated kinetic energy (IKE) (24), have been proposed as proxies for the destructive potential. It is beyond the scope of this study to make a detailed comparison with IKE, which relies on high-quality wind data that are not available for all storms. However, the surge index can be used as a method of testing how IKE-type measures reflect actual surge data. For such a comparison it would be possible to include many more additional tide-gauge records as the time frames for high-quality wind data are relatively short.

To estimate the trend in landfalling storm counts, we count the number of large surge events greater than 10 units in 1 y, which is roughly equivalent to hurricane categories 0–5. This threshold was chosen as a compromise between looking at large events and having sufficiently many events to obtain robust statistics. Since 1923 the average number of events crossing this threshold has been 5.4/y, which would increase to 9.5 events/y by 2100 were the best-fitting trend to continue (Fig. 1B). This trend is statistically significant against a null hypothesis with the same power spectrum as the input series ($P < 0.02$). We do not find a statistically significant trend in the seasonal average surge index (Fig. 1A), which by construction emphasizes the very largest events. This is because the strongest events are rare, and hence a longer time series is needed before a robust trend emerges. The same issues make it more difficult to detect trends in counts of major landfalling hurricanes (or PDI or ACE), compared with counts of all tropical storms.

As we are primarily interested in extreme events, it is constructive to examine the changes to the entire surge index probability density function (pdf). We split the surge index into cold and warm years (Fig. 1D) and compare the derived return periods (*Methods*) for the two subsets (Fig. 3). It is clear that events with annual return periods (reciprocal frequency) are significantly more intense in warm years than in cold years. We can therefore

conclude that the surge index distribution is not stationary. For rarer events (with return periods greater than 1 y) the confidence intervals from the warm and cold years overlap, which makes it difficult to visually assess whether the difference is significant. We address this by fitting generalized extreme value (GEV) distributions (*Methods*) to the cold and warm year data separately in Fig. 3. It is evident that the GEV distribution fits the surge index data, but that there are significant differences between the GEV parameters describing the warm and cold years. Both GEV fits give return periods that are consistent with the 9- to 30-y period for US coastal Katrina-magnitude events estimated from HURDAT (25). We observe that warm years are more active than cold years and that the relative difference in frequency is greatest for the most extreme events. The separate GEV fits suggest that events of Katrina magnitude are approximately two times more frequent in the warm years than in cooler
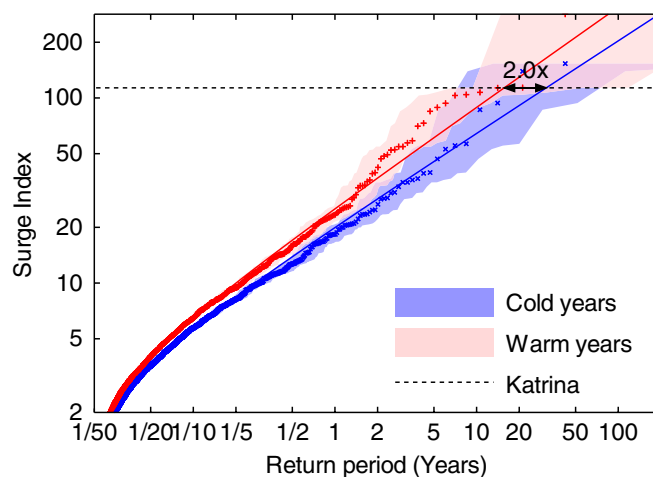
Fig. 3. Return period plot of surge index distribution for cold (blue) and warm (red) years separately (Fig. 1D). The crosses and shaded bands show return periods and confidence intervals estimated from the empirical cdf (*Methods*). Solid lines show best-fitting GEV distributions (*SI Methods, section S3*). The maximal surge index during hurricane Katrina in 2005 is shown as a dotted line.
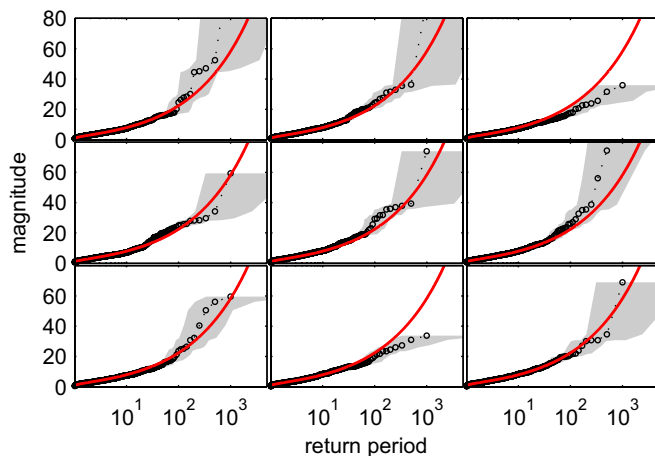
Fig. 4. Each subplot shows an example of empirical return periods (circles) and associated 5–95% confidence intervals (horizontal extent of gray band) estimated from 1,000 random samples generated with a prescribed distribution (red). The random samples were drawn from a GEV distribution with parameters $k = 0.4$, $\sigma = 1.5$, and $\mu = 2.5$. Units are arbitrary.

years (Fig. 3). This increase is significant at the 98% confidence level (*Methods*). The doubling is higher but compatible with earlier estimates from Elsner et al. (25), who reported an 11% increase (with no uncertainty estimate). We emphasize that not all events of Katrina magnitude will have equally devastating impacts. The results are also consistent with the low-resolution 1,500-y overwash sediments from landfalling Atlantic cyclones (6) that showed 40-y smoothed cyclones counts varying by about 50% while global temperatures varied by about 1 °C.

We have constructed a homogeneous surge index on the basis of instrumental records from six long tide-gauge records. We demonstrate that the surge index correlates with other measures of Atlantic cyclone activity and that it responds in particular to major landfalling cyclones. The surge index can be used to identify and estimate potential remaining biases in other records of cyclone activity.

We detect a statistically significant increasing trend in the number of moderately large surge index events since 1923. We estimate that warm years have been associated with twice as many Katrina-magnitude events compared with cold years in the global average surface temperature record.

Methods: Empirical Return Periods and Confidence Intervals

The return period (R) of events greater than x is related to the cumulative distribution function (cdf) (c) as $R(x) = dt/(1 - c(x))$, where dt is the sampling frequency. Single storms may be manifested as broad peaks that last several days (Fig. 2), which spoils the intuitive meaning of the return period when we consider daily data. We therefore down-sample the daily surge index series to a series of weekly block maxima before estimating return periods. Weekly resolution was chosen as a trade-off between having high temporal resolution and ensuring that large storms are manifested as single peaks. This resolution proved to be sufficient down-sampling for the GEV

distribution to yield high-quality fits and the results are insensitive to further down-sampling.

Because we do not know the true cdf of the underlying process, we have to rely on the observed random sample $x_1, x_2, \ldots, x_N$. That is, we do not know the exact shape of the function $c(x)$. We can estimate $c(x_i)$ empirically from the rank of x_i within the sample (26, 27). The usual method for estimating the uncertainties of the empirical estimate is Greenwood's formula for the approximate SEs (e.g., ref. 26), which is then inflated to a confidence interval assuming that the errors are normally distributed. However, this approach fails for extreme values and for small sample sizes. For extreme percentiles it is clear that the uncertainties cannot be symmetric, and the uncertainty distribution must be bounded as we know there can be no values outside the 0th- to 100th-percentile range. As we are particularly interested in extreme events, we have developed an alternative robust Monte Carlo approach for determining the confidence interval of the empirical estimates of c and thus R.

We cannot draw surrogate samples according the true distribution of x as we do not know the true distribution function (c). For any random sample (x_i) from c, the corresponding value of $c(x_i)$ will have uniform probability in the interval 0–1 by construction.

So, although we cannot draw samples according to the true process distribution, we can draw samples according to the true distribution of $c(x)$ simply by using a standard uniform random number generator. The goal is to compare this true $c(x)$ with what the empirical estimator of c would give. The difference between the true and estimated percentiles can be used to infer confidence intervals if we ensure that the empirical estimator is equivalent to the one applied to the observed sample. The empirical estimator for c (x_i) is dependent only on the rank of x_i within the sample and on the size of the sample; i.e., it is independent of the distribution, and the rank of $c(x_i)$ will be the same as the rank of x_i. We can therefore apply the empirical estimator directly to a surrogate sample of true percentiles. To summarize, the Monte Carlo procedure for determining the spread in empirical estimates of c is as follows:

i) Generate a set of N random samples from a uniform distribution between zero and one. Label this $c_{surrogate,true}$.
ii) Estimate c empirically from $c_{surrogate,true}$. Label this $c_{surrogate,empirical}$.
iii) Repeat steps *i* and *ii* many times.
iv) The confidence interval of an empirical estimate of the percentile can be determined from the spread of all of the $c_{surrogate,true}$ with the given value $c_{surrogate,empirical}$.

In Fig. 4 we show the viability of the empirical procedure on artificial data with known characteristics.

This Monte Carlo approach is more robust, conservative, and flexible than the traditional Greenwood's equation (26). Further, serial dependence, clustering, and measurement noise can be taken into account in the Monte Carlo approach by designing appropriate noise models. The normalized surge series show only very weak autocorrelation, so we fit a second-order autoregressive (AR) noise model. The AR noise is then transformed to a uniform distribution. We find that the confidence intervals are not sensitive to the serial correlation for the data used in this study.

1. World Weather Research Programme (2007) *Proceedings of the Sixth WMO International Workshop on Tropical Cyclones* (IWTC-VI) (World Meteorological Organization, Geneva, Switzerland), WMO TD No. 1383. Available at http://www.aoml.noaa.gov/hrd/Landsea/WWRP2007_1_IWTC_VI.pdf.
2. Emanuel K (2005) Increasing destructiveness of tropical cyclones over the past 30 years. *Nature* 436(7051):686–688.
3. Vecchi GA, Swanson KL, Soden BJ (2008) Climate change. Whither hurricane activity? *Science* 322(5902):687–689.
4. Jagger TH, Elsner JB (2006) Climatology models for extreme hurricane winds near the United States. *J Clim* 19:3220–3226.
5. Gray WM (1984) Atlantic seasonal hurricane frequency. Part I: El Niño and 30 mb quasi-biennial oscillation influences. *Mon Weather Rev* 112:1649–1668.
6. Goldenberg SB, Landsea CW, Mestas-Nunez AM, Gray WM (2001) The recent increase in Atlantic hurricane activity: Causes and implications. *Science* 293(5529): 474–479.
7. Mann ME, Woodruff JD, Donnelly JP, Zhang Z (2009) Atlantic hurricanes and climate over the past 1,500 years. *Nature* 460(7257):880–883.
8. Moore JC, Grinsted A, Jevrejeva S (2008) Gulf stream and ENSO increase the temperature sensitivity of Atlantic tropical cyclones. *J Clim* 21:1523–1531.
9. Villarini G, Vecchi GA, Smith JA (2010) Modeling the dependence of tropical storm counts in the North Atlantic basin on climate indices. *Mon Weather Rev* 138: 2681–2705.
10. Gray WM (1990) Strong association between West African rainfall and U.S. landfall of intense hurricanes. *Science* 2A9:1251–1256.
11. Landsea CW (2007) Counting Atlantic tropical cyclones back to 1900. *Eos Trans AGU* 88:197.
12. Knutson TR, et al. (2010) Tropical cyclones and climate change. *Nat Geosci* 3:157–163.
13. Harris DL (1963) *Characteristics of the Hurricane Storm Surge*, Technical Paper No. 48 (US Department of Commerce, Weather Bureau, Washington, DC). Available at www.csc.noaa.gov/hes/images/pdf/CHARACTERISTICS_STORM_SURGE.pdf.

14. University of Hawaii Sea Level Center (2010) RQDS and GLOSS/CLIVAR data (University of Hawaii Sea Level Center, Honolulu, Hawaii). Available at http://ilikai.soest.hawaii.edu/uhslc/. Accessed July 8 and December 6, 2012.

15. National Oceanic and Atmospheric Administration (2010) Mayport preliminary water level data (and tidal model). Available at http://tidesandcurrents.noaa.gov. Accessed December 8, 2010.

16. Pugh DT (1987) *Tides, Surges and Mean Sea Level* (Wiley, New York).

17. Jevrejeva S, Grinsted A, Moore JC, Holgate S (2006) Nonlinear trends and multi-year cycles in sea level records. *J Geophys Res* 111:C09012.

18. Jarvinen BR, Neumann CJ, Davis MAS (1984) *A Tropical Cyclone Data Tape for the North Atlantic Basin, 1886-1983: Contents, Limitations, and Uses* (National Hurricane Center, Miami, FL), NOAA Technical Memorandum NWS NHC 22. Available at www.aoml.noaa.gov/general/lib/lib1/nhclib/nwstechmemos/techmemo22.pdf.

19. Bell GD, et al. (2000) Climate assessment for 1999. *Bull Am Meteorol Soc* 81:S1–S50.

20. Gray WM, Landsea CW, Mielke PW, Berry KJ (1994) Predicting Atlantic basin seasonal tropical cyclone activity by 1 June. *Weather Forecast* 9:103–115.

21. Pielke RA, Jr., et al. (2008) Normalized hurricane damages in the United States: 1900–2005. *Nat Hazards Rev* 9(Issue 1):29–42.

22. Kocin PJ, Schumacher PN, Morales RF, Uccellini LW (1995) Overview of the 12–14 March 1993 superstorm. *Bull Am Meteorol Soc* 76:165–182.

23. Hansen J, Ruedy R, Sato M, Lo K (2010) Global surface temperature change. *Rev Geophys* 48:RG4004. Available at www.giss.nasa.gov/data/update/gistemp/.

24. Powell MD, Reinhold TA (2007) Tropical cyclone destructive potential by integrated kinetic energy. *Bull Am Meteorol Soc* 88:513–526.

25. Elsner JB, Jagger TH, Tsonis AA (2006) Estimated return periods for Hurricane Katrina. *Geophys Res Lett* 33:L08704.

26. Kaplan EL, Meier P (1958) Nonparametric estimation from incomplete observations. *J Am Stat Assoc* 53:457–481.

27. Makkonen L (2006) Plotting positions in extreme value analysis. *J Appl Meteorol Climatol* 45:334–340.

ENVIRONMENTAL SCIENCES

Supporting Information

Grinsted et al. 10.1073/pnas.1209542109

SI Methods

S1. Construction of the Surge Index. The selection criteria for the six tide gauges used in the construction of the surge index are presented in the main text. Here we summarize the steps involved in our calculation of the surge index.

i) For each station we do the following:
   a) Apply a 24-h smoothing to the hourly series, thus obtaining a moving average daily average sea-level series. Gaps shorter than 3 h are in-filled by linear interpolation.
   b) Calculate the squared day-to-day differences from this daily sea-level series.
   c) Down-sample this series to a daily surge series, using daily block maxima.
   d) Remove the annual cycle by division. The different tide-gauge locations have different sensitivities, due to local effects such as bathymetry, and normalizing by the seasonal cycle brings the records to a common reference. The background seasonal cycle is determined from the second percentile of data within a moving 21-d-wide seasonal slice. The estimated seasonal cycle is smoothed using a 180-d-long robust loess filter with periodic boundary conditions.
   e) Decluster the record. Single storm events may cause broad peaks that last several days. We therefore remove samples that are smaller than the local 3-d maximum value.
ii) Combine the six deseasonalized surge records into a single record of daily maximum values. We allow a maximum of one station missing when calculating the maximum value. Declustering (step *i*, *e*) is ignored on the rare dates, when it would have removed data from all six stations.
iii) Rescale the final surge index containing the record of daily maximal surge values to have median = 1.

The conclusions of this paper are insensitive to minor changes in the procedure. However, the justification for our further analysis using the generalized extreme value distribution hinges on the series being approximately stationary on subannual scales. Therefore, the performance of step *i*, *d* is important. We have therefore verified that step *i*, *d* removes the kink in the distribution at frequencies corresponding to annual return periods.

Steps *i*, *a* and *i*, *b* act to remove the tidal signal and the trend. The remaining signal is completely dominated by nontidal components and primarily wind-driven changes in sea level. This can be easily verified as steps *i*, *a* and *i*, *b* can be combined into a simple finite impulse response filter and the resulting frequency response can be examined. As an example, for Mayport the modeled hourly tidal signal [from National Oceanic and Atmospheric Administration (NOAA)] has a SD of 0.50 m; applying step *i*, *a* reduces this to 0.10 m; and applying step *i*, *b* reduces this to 0.01 m. Finally, we have repeated the entire analysis but explicitly remove the tidal signal before step *i*, *a* and obtain near identical results.

There are unfortunately a few gaps in the tide-gauge records, and some of these gaps could have been caused by extreme weather. Here we compare the tide-gauge records with the Atlantic Hurricane Database (HURDAT) to determine which gaps could be caused by the passing of a storm. It is implausible that storms passing close to tide gauges were not well documented. We have chosen a few simple criteria to screen for gaps that might be related to the passing of a storm:

The data gap start must overlap the timing of the storms making landfall within a ±24-h margin.

The storm must have been within 250 km of the tide gauge at the onset of the gap.
The start of the storm must precede the onset of the data gap (allowing for a 6-h slack).

From Table S1 (and Fig. S2) we see that by these criteria only eight data gaps can possibly be related to the passing of a storm. These gaps in the tide-gauge records quite likely correspond to some large storm surges that are missing in the surge index record. We have therefore made a sensitivity test where we set the surge index at the "gap-start" dates manually to have the same magnitude as Hurricane Katrina 2005. Our results are robust to this test.

S2. Events with the Largest Surge Index. In Table S2 we show the surge index of the 50 greatest events. A surge will generally also lead to a secondary peak the following day as sea level returns toward the background level. For this reason dates are not exact. Secondary peaks within 4 d of larger peaks are excluded from this list as they are considered to be the same event. In Table S2 we have also calculated accumulated cyclone energy (ACE) and US-ACE over the week centered on the date shown. We caution against comparing the relative rank of individual events. The surge index ranking reflects the impact at the specific tide-gauge locations and therefore should not be interpreted as a storm ranking. The purpose of this list is to demonstrate that the surge index truly captures cyclone activity, rather than providing a storm severity ranking.

A few events outside the hurricane season cannot be attributed to tropical cyclones. Several of these events, however, show up in other records of extreme weather; e.g., the large March 13, 1993 event is commonly known as the 1993 superstorm (1). NOAA has an extensive record of this event.

S3. GEV Distribution Fitting. The general method of fitting a distribution (*f*), with parameters (*m*), to a series (*x*) involves maximizing the likelihood function

$$L(m) = \prod_i f_m(x_i), \qquad [S1]$$

where *i* is an index into the series *x*. In practice, this is usually done by minimizing $-\log(L)$. The method can be easily extended to nonstationary distributions by having *m* vary with time (*i*). In this study, we achieve this by letting *m* be dependent on global temperature. The calculation of *L* can easily be parallelized and for some distribution functions it may be advantageous to perform this calculation on a graphical processing unit.

The confidence intervals of the model parameters are given by the likelihood function. We sample the parameter space according to the likelihood density, using Markov chain Monte Carlo (MCMC) using the Metropolis–Hastings algorithm (2). Regions of the parameter space that are likely will be sampled with a high density whereas less likely regions will be sampled less densely. From the percentiles of the sampling density we determine the confidence intervals. In this study we denote the median of the likelihood distribution as the "best guess" that is more robust than using the maximum-likelihood model.

We verify convergence of the MCMC solutions by manual inspection of the accepted models and their autocorrelation structure. In this study, our likelihood functions are very cheap to calculate, and we can afford to make the MCMC runs much longer than is strictly necessary. We speed up convergence, by taking random steps in a linearly transformed model space chosen on the basis of a principal component analysis (PCA) of the

accepted models from an initial shorter MCMC run. We observe that the burn-in is usually confined to the shorter initial MCMC run, and that the transformed steps almost always gives near optimal rejection rates.

Under certain conditions the central limit theorem states that the sum of a set of independent random variables will approach a normal distribution in the limit of infinitely large sets. Analogously, the distribution of block maxima approaches the generalized extreme value (GEV) distribution as the blocks get larger (3). For that reason we expect that block maxima of the surge index

model block maxima: the Weibull, Frechet, and Gumbel distributions. The flexibility lets the data decide which distribution is appropriate.

It is sometimes argued (e.g., ref. 3) that taking block maxima is a wasteful method to infer statistics of extreme events. The reasoning is that there may be a small chance that two very large events are inside the same block and that taking block maxima could be discarding one of the already rare large events. The peaks-over-threshold (POT) method is the usual proposed alternative, where a distribution is fitted to all events that are

$$
f_{m=(k,\mu,\sigma)}(x) = \begin{cases} \dfrac{1}{\sigma}\left(1+k\dfrac{x-\mu}{\sigma}\right)^{-1-\frac{1}{k}} e^{-\left(1+k\frac{x-\mu}{\sigma}\right)^{-\frac{1}{k}}} & \text{for } 1+\dfrac{k(x-\mu)}{\sigma} > 0 \text{ and } k \neq 0 \\[2mm] \dfrac{1}{\sigma} e^{\frac{\mu-x}{\sigma}-e^{\frac{\mu-x}{\sigma}}} & \text{for } k=0 \\[2mm] 0 & \text{otherwise,} \end{cases} \qquad \textbf{[S2]}
$$

should follow a GEV distribution. The GEV distribution, used in this study, can be described by
where μ, σ, and k are the location, scale, and shape parameters, respectively. In the MCMC inference of the GEV model we use the conventional uniform priors on μ, $\log(\sigma)$, and k.

We are interested in the return period of large and rare events. We find that the surge index maxima of 7-d blocks can be accurately modeled by the GEV distribution over a wide range of magnitudes (Fig. 3). Sensitivity tests show that our results are not sensitive to larger block sizes. The GEV distribution is flexible and combines three simpler types of distributions commonly used to

above a certain threshold. The advantage is that no large events are discarded. The drawback of the POT approach is that return periods can be calculated only if the frequency of threshold crossing is known. The threshold return period can be estimated using empirical cumulative distribution. However, this empirical estimate assumes stationarity and the POT method is hence ill-suited for nonstationary series. For that reason we use exclusively the GEV distribution. However, our conclusions are insensitive to different block sizes and we get compatible results using POT analysis; we conclude that extreme event wastage is not an issue.

1. Kocin PJ, Schumacher PN, Morales RF, Uccellini LW (1995) Overview of the 12–14 March 1993 superstorm. *Bull Am Meteorol Soc* 76:165–182.
2. Hastings WK (1970) Monte Carlo sampling methods using Markov chains and their applications. *Biometrika* 57:97–109.

3. Coles S (2001) *An Introduction to Statistical Modeling of Extreme Values* (Springer, London).
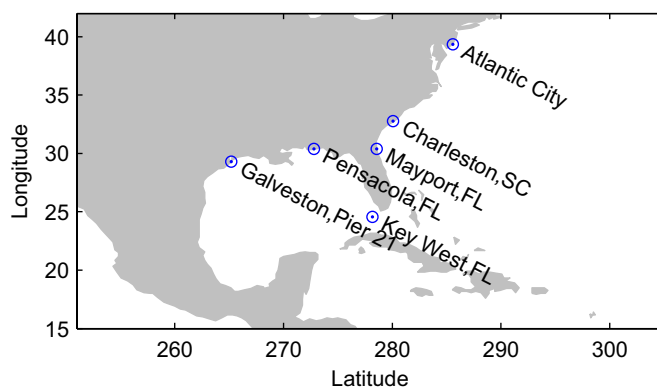
Fig. S1. Map showing locations of tide gauges used in the construction of the surge index.
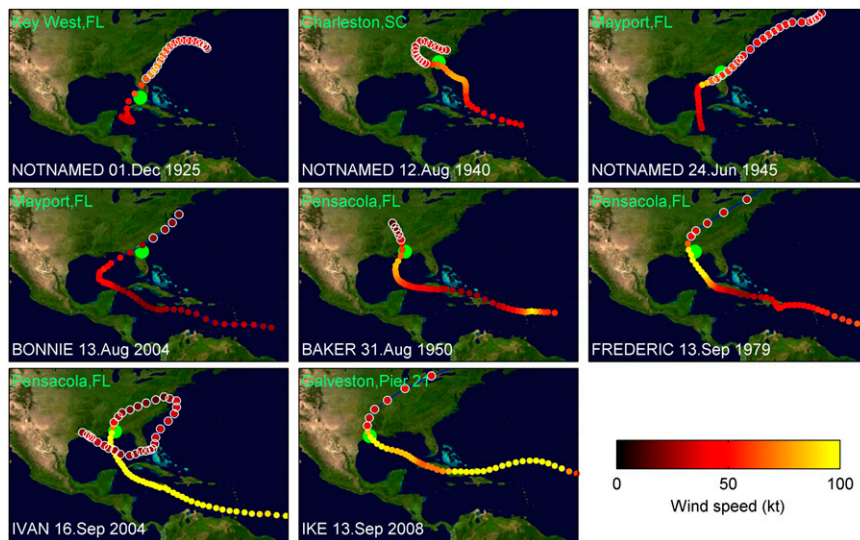
Fig. S2. Tracks of storms (blue line) that likely are the cause of gaps in the tide-gauge records. Red-yellow dots indicate wind speed at 6-h intervals; green shows tide-gauge location. White circles indicate when the tide gauge has missing data.

Table S1. Tide-gauge data gaps that coincide with storm landfall

Tide gauge	Gap start	Wind, kt	Distance, km	Storm name
Key West, FL	Dec. 1, 1925; 07:00	65	158	Not named
Charleston, SC	Aug. 12, 1940; 07:00	70	77	Not named
Mayport, FL	June 24, 1945; 03:00	95	118	Not named
Mayport, FL	Aug. 13, 2004; 06:00	45	128	Bonnie*
Pensacola, FL	Aug. 31, 1950; 14:00	83	63	Baker
Pensacola, FL	Sept. 13, 1979; 17:00	115	119	Frederic
Pensacola, FL	Sept. 16, 2004; 18:00	115	60	Ivan
Galveston, Pier 21	Sept. 13, 2008; 15:00	95	8	Ike

List of HURDAT storms that coincide with data gaps in the tide-gauge records (see text for selection criteria). "Gap start" shows the date of the first missing sample. "Wind" shows the maximum wind speed in the 24-h days preceding the gap. "Distance" refers to the closest distance to tide gauge in the 24 h centered on the gap start. *Tropical storm Bonnie had similar timing to hurricane Charley and both could be responsible for the tide-gauge outage.

Table S2. 50 greatest events

Rank	Event date	Candidate storm (category)	Surge index	ACE	US-ACE	Wind, kt
1	Sept. 20, 1926	"Great Miami hurricane" (4)	283	422,098	228,174	125
2	July 25, 1934	Not named (1)	153	39,450	39,450	65
3	Sept. 19, 1947	Not named (5)	139	223,806	223,806	130
4	Sept. 10, 1961	Carla (5)	114	588,267	312,007	125
5	Aug. 30, 2005	Katrina (5)	113	189,274	167,424	110
6	July 10, 2005	Dennis (4)	107	207,799	188,024	120
7	Sept. 12, 2008	Ike (4)	104	146,499	143,599	100
8	Sept. 10, 1965	Betsy (4)	94	169,699	169,699	135
9	Sept. 1, 1932	Not named (1)	89	172,324	65,775	70
10	June 28, 1957	Audrey (4)	86	79,474	79,474	125
11	Sept. 27, 1998	Georges (4)	85	463,173	155,699	95
12	Sept. 1, 2008	Gustav (4)	70	326,423	300,849	125
13	Oct. 6, 1995	Opal (4)	59	180,099	91,975	110
14	Aug. 5, 1940	Not named (1)	57	117,449	117,449	70
15	Aug. 18, 1969	Camille (5)	57	362,419	217,996	165
16	Aug. 13, 1932	Not named (4)	55	64,600	64,600	125
17	Oct. 25, 2005	Wilma (5)	55	190,674	161,224	110
18	July 15, 2003	Claudette (1)	55	81,050	56,875	75
19	Oct. 4, 1964	Hilda (4)	53	166,994	166,994	83
20	Sept. 15, 2004	Ivan (5)	53	406,723	364,298	105
21	Aug. 17, 1983	Alicia (3)	52	68,500	68,500	100
22	Aug. 31, 1942	Not named (3)	49	162,324	93,275	70
23	Aug. 26, 1926	Not named (3)	48	110,974	110,974	95
24	Sept. 27, 2002	Isidore (3)	47	180,174	180,174	110
25	8-Sep-1974	Carmen (4)	47	168,899	124,474	120
26	Sept. 12, 1979	Frederic (4)	42	272,524	134,274	115
27	Sept. 25, 1941	Not named (1)	40	229,774	57,725	70
28	April 8, 1938		39			
29	Sept. 19, 1928	Not named (5)	39	152,974	152,974	140
30	Feb. 27, 1984		39			
31	Sept. 30, 1959	Gracie (4)	36	281,526	104,798	96
32	Aug. 9, 1980	Allen (5)	36	345,148	345,148	100
33	Sept. 24, 2005	Rita (5)	35	253,274	222,699	100
34	March 14, 1993		35			
35	Sept. 11, 1964	Dora (3)	35	307,606	121,637	83
36	Oct. 28, 1985	Juan (1)	34	79,850	79,850	65
37	June 12, 2005	Arlene (0)	34	31,175	31,175	50
38	Feb. 25, 1965		33			
39	Sept. 2, 1985	Elena (3)	33	145,274	145,274	100
40	Aug. 3, 1933	Not named (1)	31	63,500	63,500	70
41	July 6, 1933	Not named (2)	31	118,524		70
42	July 30, 1995	Erin (1)	30	65,150	65,150	80
43	Sept. 5, 1979	David (5)	29	206,774	158,549	150
44	Sept. 22, 1948	Not named (3)	29	143,824	143,824	90
45	Oct. 19, 1944	Not named (3)	29	124,557	124,557	58
46	Oct. 5, 1949	Not named (3)	28	75,853	75,853	112
47	Dec. 7, 1969		28			
48	July 24, 1933	Not named (0)	27	69,000	69,000	40
49	Aug. 4, 1995	Erin (1)	26	68,925	68,925	80
50	Jan. 21, 1979		26			

ACE and US-ACE are calculated over the week centered at the date shown. Wind shows the maximum landfalling wind speed.